

# Control of Sequential Compartment Formation in *Drosophila*

A uniform mechanism may control the locations of successive binary developmental commitments.

Stuart A. Kauffman, Ronald M. Shymko, Kenneth Trabert

Among the most fundamental tasks faced by the developing embryo is the reliable assignment of different developmental programs to the proper regions of the embryo. In many different organisms the fate of any region becomes progres-

sively restricted. Recent discoveries indicate that in *Drosophila melanogaster* this is manifested by the formation of lines of clonal restriction, called compartmental boundaries (1-7), which arise sequentially and subdivide the egg into discrete regions in the earliest stages of embryogenesis. Later, additional lines subdivide imaginal discs, the larval anlagen that metamorphose into the different adult appendages. The sequence and geometries of these lines almost certainly reflect the order in which discrete spatial domains assume different developmental programs, and provide information about the underlying positional cues which delineate and trigger those commitments. Our purpose in this article is

to discuss a simple dynamical model, that appears able to generate reliably the known sequence and geometries of compartmental boundaries in *Drosophila*, and to induce the proper developmental program in each region.

---

**Summary.** During development of *Drosophila melanogaster*, sequential commitment to alternative development programs occurs in neighboring groups of cells. These commitments appear to be reflected by lines of clonal restriction, called compartmental boundaries, which progressively subdivide the early embryo, and later the imaginal discs, which give rise to different adult appendages. We propose that a reaction-diffusion system acts throughout development and generates a sequence of differently shaped chemical patterns. These patterns account for the sequence and geometries of compartmental boundaries, and predict that each terminal compartment is specified by a unique combination of binary choices made during its formation. This binary "code" interprets coherently the patterned metaplasia seen in transdetermination and homeotic mutations.

---

sively restricted. Recent discoveries indicate that in *Drosophila melanogaster* this is manifested by the formation of lines of clonal restriction, called compartmental boundaries (1-7), which arise sequentially and subdivide the egg into discrete regions in the earliest stages of embryogenesis. Later, additional lines subdivide imaginal discs, the larval anlagen that metamorphose into the different adult appendages. The sequence and geometries of these lines almost certainly reflect the order in which discrete spatial domains assume different developmental programs, and provide information about the underlying positional cues which delineate and trigger those commitments. Our purpose in this article is

*Drosophila melanogaster* is a holometabolous insect. At 25°C the egg hatches about 24 hours after oviposition, the three larval instars last a total of about 4 days, pupariation and metamorphosis require about 4 days, and the adult lives several weeks. After fertilization, the zygotic nucleus undergoes 12 or 13 rapid mitoses without division of the ellipsoidal egg, thereby creating a syncytium (8). By the ninth cleavage, nuclei move outward to the cortex of the egg. After the 13th cleavage, at about 3 hours, division temporarily ceases, and cell membranes separate the cortical nuclei, creating the cellular blastoderm. About 20 minutes later gastrulation takes place, and cell division commences.

Direct evidence shows that the nuclei of the blastoderm are still totipotent, but that these initial cells are already determined at least into anterior and posterior zones (9). Additional evidence (10) strongly suggests that, at about this time, small nests of cells in different regions of

the blastoderm are set apart from the forming larval structures, and become the imaginal discs. Slightly later, each disc is "determined" to form a particular part of the adult epidermis during metamorphosis. There are the following pairs of discs: eye-antenna, labial, clypeo-labrum, humeral, first leg, second leg, third leg, wing, haltere, abdominal histoblasts and the single bilaterally fused genital disc. During larval development the discs grow to 10,000 to 40,000 cells (10). During metamorphosis, most larval structures lyse, and the ectoderm of the adult is formed by the terminal differentiation and eversion of the imaginal discs.

Using gynandromorphs to construct a fate map of the egg showing the locations of regions that will give rise to each imaginal disc (11), and with the use of gynandromorphs and mitotic recombination (10), it has been possible to establish that the initial determination processes subdivide the egg into a number of geometric domains, in each of which a group of cells related by spatial proximity, but not clonal ancestry, becomes determined to form a specific imaginal disc.

The discovery of the sequential formation of lines of clonal restriction rests on the genetic technique of mitotic recombination (10). A larva that is a heterozygote for a recessive gene, such as *mwh* (multiple wing hairs), is phenotypically normal. Irradiation of the larva during development can cause a somatic recombination event in a G<sub>2</sub> stage cell, leading to the formation of two daughter cells, one of which is homozygous *mwh*, the other homozygous for the wild-type *mwh* allele. The homozygous *mwh* cell continues to divide, generating a clone. After metamorphosis, the clone is visible as an extended *mwh* patch on the adult cuticle. The size, shape, and location of the clone reflect features of its history.

## Operational Definition of Developmental Compartments

Mitotic recombination events resulting in marked clones can be induced by irradiation as early in development as the cellular blastoderm stage. Garcia-Bellido and co-workers (1, 2) found that clones initiated at such early stages occur at arbitrary locations on the adult wing, except that they never cross a specific line on the adult surface, even though the border of such a clone might run along that line for hundreds of cells. This line divides the wing and mesothorax into anterior and posterior regions. The clones

---

Dr. Kauffman is an associate professor and Dr. Shymko is a postdoctoral fellow in the Department of Biochemistry and Biophysics, School of Medicine, University of Pennsylvania, Philadelphia 19174. Dr. Trabert was a research assistant in the Laboratory of Theoretical Biology, National Cancer Institute, National Institutes of Health, Bethesda, Maryland 20014, and is now at the Environmental Protection Agency in Washington, D.C.

behave as though they were “respecting” the line. This line of clonal restriction provides the operational definition of a compartmental boundary separating the anterior and posterior compartments of the wing and thorax (Fig. 1).

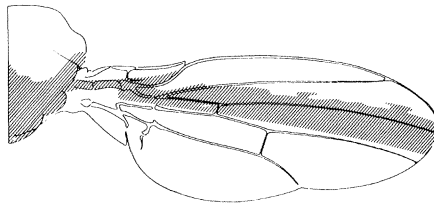


Fig. 1. A large clone whose posterior margin runs along the anterior-posterior border of the wing and thorax. [From Garcia-Bellido *et al.* (2)]

### Sequential Compartmentalization of the Early Embryo

Steiner (4), Wieshaus and Gehring (5), and Lawrence and Morata (12) have induced clones at the blastoderm stage and found that no clones cross between the adjacent prothorax, mesothorax, or metathorax structures, or between the corresponding prothoracic, mesothoracic, or metathoracic legs. Steiner (4) also found that no clone crossed between the anterior and posterior halves of each leg. Therefore it appears that lines of clone restriction separate the three thoracic segments, and even subdivide each of these into anterior and posterior compartments, by the blastoderm stage. However, clones induced at the same stage do cross from wing to mesothoracic leg, from metathorax to metathoracic leg, and from left to right prothoracic leg (4, 5, 12).

Lawrence and Morata (12) found that clones induced a few hours after the blastoderm stage no longer crossed from wing to mesothoracic leg. These data demonstrate that lines of clone restriction subdivide the blastoderm longitudinally prior to the establishment of restriction lines separating the dorsal (prothorax, mesothorax, metathorax) discs from the ventral (leg) discs. It seems clear that lines of clone restriction arise sequentially as the egg matures past the blastoderm stage, and progressively isolate the groups of cells that comprise the initial imaginal disc anlagen.

### Sequential Compartmentalization in the Wing Disc

The anterior-posterior compartmental boundary subdivides the wing disc by the blastoderm stage (1, 2). Clones marked at later stages of development always respect this boundary. However, Garcia-Bellido and co-workers have discovered in the wing disc that further compartmental boundaries are formed in a specific sequence and at specific stages of development. Among flies irradiated prior to the formation of each compartmental boundary, some clones will be seen crossing that boundary; in flies irradiated after the formation of the

boundary, no clones will be seen straddling that line.

The observed compartments and their times of appearance are: (i) anterior-posterior at about 3 to 10 hours; (ii) dorsal-ventral at about 30 to 40 hours; (iii) wing-thorax at about 30 to 40 hours; (iv) scutum-scutellum, and postscutum-postscutellum at about 70 hours; (v) proximal-distal wing at about 96 hours.

Data for the occurrence and timing of the later compartments in the wing disc are less secure than for the earlier compartments, both because good surface markers are sparse in some areas of the wing and thorax, and because clones marked late in development are small, making compartmental boundaries harder to observe. To overcome the latter problem, Morata and Ripoll (13) introduced and Garcia-Bellido *et al.* (1, 2) made use of flies heterozygotic for a mutant gene, *Minute*,  $M/M^+$ . *Minute* flies develop more slowly than wild-type flies. Irradiation produces some  $M^+/M^+$  cells which grow faster than  $M/M^+$  cells, thereby creating large clones which “fill up” most of a compartment and help establish its boundaries. Because of uncertainties about the relative developmental ages of *Minute* heterozygotes and wild-type flies, the timing of later compartmental boundaries is only approximate.

The five compartmental boundaries are shown schematically in Fig. 2a. In Fig. 2b they are shown projected onto the fate map of the third instar wing disc (14). During metamorphosis, the wing disc “folds” along the dorsal-ventral line, and apposes dorsal and ventral thorax, while the wing everts.

Projecting the successive compartmental lines onto the mature third instar disc (Fig. 2b) may not accurately reflect their detailed geometries on the growing disc at the times the lines were first formed. In fact, the first anterior-posterior boundary is actually present on the blastoderm (4, 5) before the wing and mesothoracic leg are clonally isolated and simultaneously divides wing and leg into anterior and posterior compartments. The remaining four boundaries

form on the wing disc proper as it grows and changes shape. Each of the first three boundaries successively bisects all the compartments created by the earlier lines. The last two each seem simultaneously to bisect two or more previous compartments. Garcia-Bellido *et al.* (2) point out the astonishing anterior-posterior and dorsal-ventral (that is, twofold) symmetries of the process. Indeed, the only deviation from complete twofold symmetry is the lack, at the fourth compartmentalization, of a line bisecting ventral thorax. But, in fact, that line may well exist, for Garcia-Bellido *et al.* (2) happened only to look in the dorsal thorax at that time.

If wing disc compartmental boundaries separate groups of cells with different developmental commitments, then the geometries of the lines suggest that a terminal wing disc compartment is specified by a unique combination of binary names; for example, *anterior*, not posterior; *dorsal*, not ventral; *wing*, not thorax; *proximal*, not distal.

### Different Compartments Appear to Have Different Commitments

At least some lines of clone restriction almost certainly separate groups of cells with distinct developmental commitments. The different imaginal discs are in different states of determination. Determination is operationally defined as a clonally heritable state (10); therefore, determination of groups of cells to one or another disc implies clonal isolation of each group. Since neighboring domains on the blastoderm become determined to form different imaginal discs, such alternate commitments almost certainly generate the lines of clone restriction which sequentially subdivide the early embryo.

Compartmental boundaries subdividing the wing disc also seem to separate domains of cells carrying different developmental commitments. In this case, the criterion of clonal heritability cannot be applied since, during culture of disc fragments, regeneration across wing compartmental boundaries can occur (15). However, in several homeotic mutants, which convert one disc or disc region to the commitment of another disc or disc region, the boundaries of action of the mutants coincide with the boundaries of wing compartments (16, 17). This suggests that a homeotic gene can have a compartment as its domain of action, and that intradisc compartments are distinctly committed cell populations (1, 17).

Some apparent lines of clone restric-

tion may not separate domains of distinctly committed cells. Most critically, mere clonal isolation itself can never prove that the two isolated populations of cells are different. For example, a line of cell death might isolate two subpopulations of identical cells. Apparent lines of clone restriction might be artifacts because of the fusion of initially separated regions of cells spanned by early large clones, but not late small clones; or because late clones are small and unlikely to span between distant structures. However, use of large  $M^+$  clones in *Minute* heterozygotes obviates most of the latter problems; and it appears likely that, in most cases, a compartmental boundary does divide a contiguous group of cells, as hypothesized by Garcia-Bellido *et al.* (2) and Crick and Lawrence (7).

The data now available indicate that compartmental lines arise sequentially throughout development from the earliest stages of embryogenesis and progressively subdivide and isolate groups of cells spatially, probably as a reflection of the sequential commitment of neighboring groups of cells to alternative developmental fates. Thus we could consider that a uniform mechanism might act throughout development to account for the number, position, symmetries, and sequence in which compartmental boundaries form. We propose a model that appears able to do so, a model that provides an explicit measure of the similarity of developmental programs in different compartments. Since the lines on the wing disc are the best established, we first construct our model for the wing, then apply it to other discs and early embryo.

### Characteristic Chemical Patterns

We postulate a single biochemical system of two components, with concentrations  $X(\mathbf{r}, t)$ ,  $Y(\mathbf{r}, t)$ , at position  $\mathbf{r}$ , time  $t$ , which are being synthesized and destroyed at rates  $F(X, Y)$  and  $G(X, Y)$ , and which are diffusing throughout the tissue. The equations for this system are:

$$\begin{aligned} \frac{\partial X}{\partial t} &= F(X, Y) + D_1 \nabla^2 X \\ \frac{\partial Y}{\partial t} &= G(X, Y) + D_2 \nabla^2 Y \end{aligned} \quad (1)$$

Biochemical dynamical systems such as Eqs. 1 can exhibit a variety of behaviors. In particular, as shown long ago by Turing (18) and recently by Gmitro and Scrivin (19) and Meinhardt (20), and reviewed by Nicolis and Prigogine

(21), such a system can have the property that its spatially uniform steady state,  $X = X_0$ ,  $Y = Y_0$  [defined by the simultaneous solution of  $F(X_0, Y_0) = 0$ ,  $G(X_0, Y_0) = 0$ ] is stable to all spatially distributed perturbations except those perturbations whose spatial wavelengths fall in a narrow range around some specific, characteristic wavelength,  $l_0$ . Perturbations with wavelengths outside this range will decay to the spatially homogeneous steady state; perturbations above and below the steady state concentrations,  $X_0, Y_0$ , with wavelengths near the natural chemical wavelength,  $l_0$ , will grow in amplitude and create a spatially inhomogeneous pattern of chemical concentrations. If the reaction functions  $F(X, Y)$ ,  $G(X, Y)$  are linear, the amplitude of such a wave pattern grows without bound. However, with appropriate nonlinear reaction functions  $F(X, Y)$ ,  $G(X, Y)$  all such perturbations will either decay or grow to a maximum amplitude without oscillations in time. Therefore, this system has the capability of establishing

stable, steady state spatial patterns of concentration with spatial wavelength equal to  $l_0$ . Given expected values of diffusion constants of about  $10^{-7}$  to  $10^{-5}$   $\text{cm}^2/\text{sec}$ , such dynamical systems typically have natural chemical wavelengths on the order of 50 to 150  $\mu\text{m}$  (22). This is appropriate for the size of developing imaginal discs. A biochemical kinetic system exhibiting these properties, and the mathematical analysis of Eqs. 1 is given in the appendix.

Thermal noise continuously introduces small local fluctuations to the spatially uniform steady state. These can be decomposed into a Fourier series, a weighted sum of very many spatial wavelengths. Thus, thermal noise guarantees that some very small amplitude wavelength equal to  $l_0$  is present. The dynamical system acts as a filter and will select and amplify that wave in time while all other wavelengths are suppressed, creating a stationary spatial pattern of wavelength  $l_0$ . This was the heart of Turing's model (18) for the spontaneous formation of a chemical pattern from a spatially homogeneous state.

### Reactions in a Growing Domain Create a Sequence of Patterns

A critical feature of compartmental boundaries is that they arise in a well-defined sequence as the imaginal disc grows in size. Our Eqs. 1 support only chemical patterns with wavelengths equal to  $l_0$ . Let this chemical system occur in a closed bounded domain; and assume that there is no flux of reactants  $X$  and  $Y$  through the boundaries. Since diffusion occurs down spatial gradients of concentration, this assumption imposes the mathematical boundary condition that the spatial gradient of concentration at the boundaries be flat along lines perpendicular to the boundaries (23). If, for example, the chemical system is in a one-dimensional domain of length  $L$ , the no-flux boundary condition constrains the spatial patterns that appear to be superpositions of one or more sinusoidally shaped functions of the form  $\cos(n\pi r/L)$ , ( $n = 1, 2, 3, \dots$ ,  $0 \leq r \leq L$ ), which have zero spatial derivative, and consequently local maxima or minima, at the boundaries  $r = 0$  and  $r = L$ . The  $n^{\text{th}}$  of these patterns has wavelength  $2L/n$ ; if this pattern is present,  $n$  half-waves of length  $L/n$  fit into the domain of length  $L$ . However, our chemical system (Eqs. 1) only allows chemical patterns of one wavelength,  $l_0$ , to grow. Therefore, the boundary conditions can be satisfied and patterns can appear only when the length of

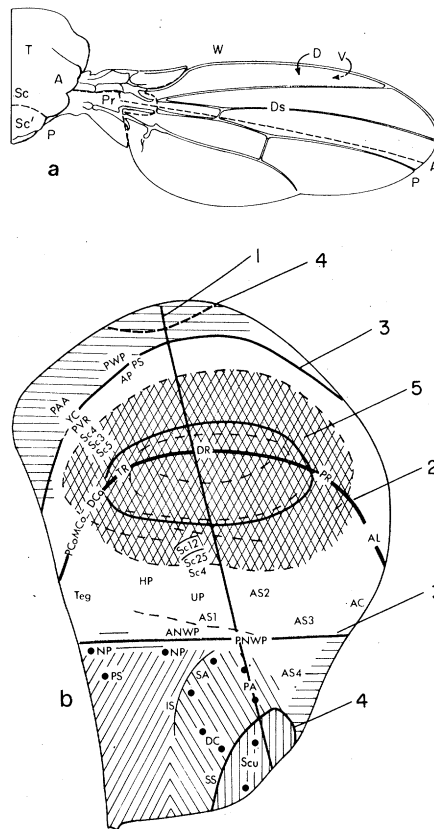


Fig. 2. (a) The five compartmental lines on the thorax and wing. A, anterior; P, posterior; V, ventral; D, dorsal; T, thorax; W, wing; Pr, proximal wing; Ds, distal wing; Sc, scutum; Sc', scutellum. [From Garcia-Bellido (1)] (b) Projection of the five compartmental boundaries onto the fate map [Bryant (14)] of the third instar wing disc. The dotted line 4 is the postulated compartmental line in the ventral thorax needed to complete the anterior-posterior, dorsal-ventral (twofold) symmetry.

the one-dimensional domain  $L$  is an integral multiple of the half-wavelength  $l_0/2$ ; that is,  $L = nl_0/2$ .

Now suppose the length  $L$  of the one-dimensional domain is less than  $l_0/2$ . No pattern of wavelength  $l_0$  can "fit" into this length, hence no pattern can emerge. The chemical system stays at its spatially homogeneous steady state. Let the "tissue" length gradually increase. When  $L = l_0/2$  the first chemical pattern, in which one half-wavelength fits into the length  $L$ , will grow, with a maximum of concentration at one boundary and a minimum at the other boundary.

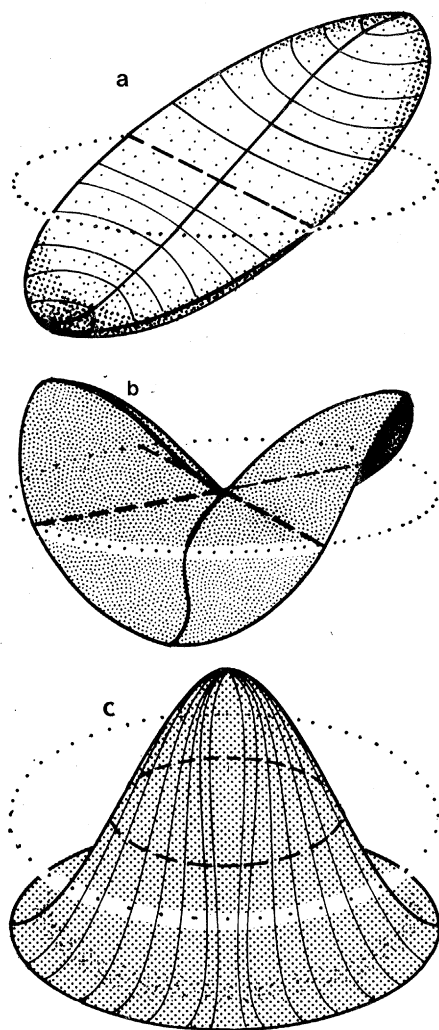


Fig. 3. (a) Wave pattern generated on a circle with scaled radius  $kr = 1.82$ . The pattern is the product of a radial part,  $J_1(kr)$  [the first order Bessel function (26)] and an angular part,  $\cos \phi$ . The dashed nodal line of zero (that is, steady state) concentration runs along the diameter of the circle from  $\phi = 90^\circ$  to  $\phi = 270^\circ$ . The dotted circle outlines the circular radius. (b) Wave pattern,  $J_2(kr) \cos 2\phi$ , generated at a scaled radius of 3.1. The dashed lines are crossed nodal lines on two perpendicular diameters. (c) Pattern generated at a scaled radius of 3.8, where the zero in the derivative of  $J_0(kr)$  matches the radial boundary condition. The pattern is  $J_0(kr) \cos 0\phi$ , which has no angular variation. The nodal line is concentric with the outer radius.

As the length of the tissue increases beyond  $L = l_0/2$  the first pattern will no longer fit, and will decay back to the homogeneous steady state. When the tissue grows to  $L = l_0$ , an entire cosine pattern, maximal at both ends and minimal in the middle, or vice versa, arises. In general, at length  $L = nl_0/2$ ,  $n$  half-wavelengths fit into the domain in tandem. Thus at a discrete succession of lengths  $L = l_0/2, l_0, 3l_0/2, \dots, nl_0/2$  distinct sinusoidal chemical patterns emerge and decay.

### Nodal Lines of Sequential Patterns Create Compartments

In direct analogy to the one-dimensional case, chemical system (Eqs. 1) will produce a sequence of differently shaped chemical patterns on complex, growing surfaces such as the wing disc. The exact shape history of the wing disc is not yet known in detail (24), but by mid-first instar it is a single-cell layer backed by a thin peripodial membrane. We will therefore approximate it as a planar shape. Since the wing disc is only joined to the larva by a stalk, a natural assumption is that no flux of  $X$  and  $Y$  occurs across the edge of the disc into the hemolymph.

On a growing two-dimensional domain, the shapes of the chemical patterns that arise depend on both the size and shape of the domain. For example, on a growing circular imaginal disc, the first three patterns that arise are shown in Fig. 3, a to c. As we describe below, distortion from a circle to an ellipse distorts the shapes of the chemical patterns.

The chemical patterns that form provide a means for drawing a succession of compartmental lines across the disc. Since compartmental lines appear to reflect the commitments of the divided groups of cells to two alternative fates, it is natural to assume that each of the chemical patterns induces cells in different regions of the disc to adopt one of two different commitments. The steady state concentrations,  $X_0$  and  $Y_0$ , occur as the nodal lines of each chemical pattern, dividing the disc into alternate regions with concentrations above and below the steady state (Figs. 3, a to c). Therefore we suppose  $X_0$  is the threshold concentration of a morphogen, inducing one binary commitment (for example, anterior) in cells above threshold, and the alternate commitment (posterior) in cells below threshold and that this commitment is recorded by a two-state memory switch or on-off "selector gene" (1) in each cell.

Our model postulates a succession of

differently shaped chemical patterns that grow and die away. The two-state switch recording the "anterior" or "posterior" decision in each cell provides a memory device for the location of the first line, which can thereafter decay. A different two-state switch would be required for the compartment boundary induced by each successive pattern, the first recording "anterior" or "posterior"; the second recording "dorsal" or "ventral"; the third "wing" or "thorax." The sequential activation of each binary switch by the successive formation of boundaries would therefore create a binary combinatorial "code word" specifying each terminal compartment. We discuss this below.

Each chemical pattern can arise in either of two orientations, since concentrations on one side of a nodal line could be above or below threshold. To break this symmetry, we must suppose that some inhomogeneity properly orients each chemical pattern. For example, the stalk of the disc might play such a role. An important further implication of the assumption of a single threshold  $X_0$  is that, in a given chemical pattern, more than one nodal line might simultaneously divide the domain, creating more than one compartmental boundary, but only the two possible switch states would be induced alternately (+, -, +, ...) in the neighboring regions with concentrations above and below  $X_0$ . If, in *Drosophila*, more than one compartmental line simultaneously arises, then more than two commitments might conceivably have been chosen. For example, the wing-thorax boundary (Fig. 2b) seems to arise as a pair of lines separating the disc into three regions. Our model assigns identical states to the two ends of the disc and the alternate state to the middle. It is interesting that, behaviorally, the two ends are thoracic and the middle is wing.

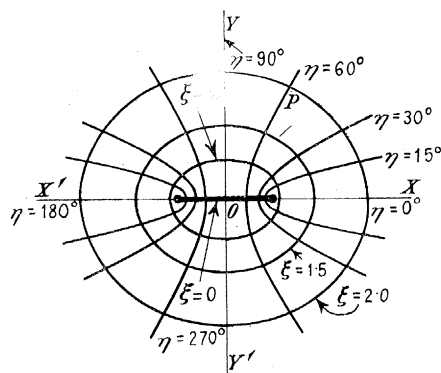


Fig. 4. The coordinates of an ellipse,  $\xi$  and  $\eta$ , are constant on confocal ellipses and hyperbolae, respectively. The interfocal distance is  $2h$ .

Any model of compartmentalization requires a mechanism by which clones "respect" the lines. Morata and Lawrence (17) and we propose that the alternate commitments create distinct cell affinity properties on the two sides of each line such that local cell sorting maintains the clonal integrity of compartment lines. Local sorting is consistent with the observation that marked clones remain coherent.

### Chemical Patterns on an Ellipse Fit the Sequence on the Wing

As was noted earlier, the first, anterior-posterior, compartment line is formed on the blastoderm and must be explained in the context of the ellipsoidal geometry of the surface of the egg. We show below that our model accounts for this first boundary. The dorsal-ventral, wing-thorax, scutum-scutellum, and proximal-distal compartment lines arise on the wing disc itself and should closely match the lines predicted by our model on an appropriate geometry. Two factors dictate the choice of an ellipse for our approximation instead of, for example, a circle (Fig. 3, a to c). First, throughout larval life the true wing disc is more similar to an ellipse than to a circle (24). Second, the ellipse is the most complex

planar figure for which the succession of chemical patterns can be investigated analytically; thereafter, detailed simulations or other approximation techniques become necessary.

On the circle, the nodal lines form along the radii and along the concentric circles. That is, the model compartmental lines run along lines that are the natural coordinate system for the circle. On an ellipse, the natural coordinate system (25) (Fig. 4) consists of concentric ellipses rather than concentric circles, and pairs of confocal hyperbolae rather than radii. Thus, on an ellipse, model compartmental boundaries form along these lines. As the ellipse grows, the modes that occur are given by products of cosine- or sine-elliptic Mathieu functions (25, 26, 27) of the form  $Ce_n(\xi, s_{n1})ce_n(\eta, s_{n1})$  or  $Se_n(\xi, s_{n1})se_n(\eta, s_{n1})$ , which we abbreviate  $Ce_n$  or  $Se_n$  (see appendix for explanation of the symbols). For most of the modes we consider,  $j = 1$ , and therefore we use the further abbreviations  $Ce_n$  or  $Se_n$  for the above modes when  $j = 1$ .

The elongation of an ellipse, relative to a circle, confers two preferred axes, the major and minor. This serves to orient successive wave patterns in contrast with the random orientation of successive patterns on the circle. The first pattern to fit on is a distortion of the first

pattern on a circle, and not surprisingly for a dynamic system with a preferred wavelength, it fits on the long way first (Fig. 5A) (28). This wave pattern is a product of first cosine-elliptic functions,  $Ce_1(\xi, s_{11})ce_1(\eta, s_{11})$ , or  $Ce_1$  in our notation. Figure 5, A to F, show the succession of characteristically shaped patterns. The solid lines are the anti-symmetry nodal lines corresponding to postulated "threshold" compartmental lines. The succession of modes is  $Ce_1$  (Fig. 5A),  $Se_1$  (Fig. 5B),  $Ce_2$  (Fig. 5C),  $Se_2$  (Fig. 5D),  $Ce_3$  (Fig. 5E), and  $Ce_0$  (Fig. 5F).

The first elliptical mode,  $Ce_1$  (Fig. 5A), has a nodal line along the minor axis of the elliptical disc which draws the first boundary on the disc proper, the dorsal-ventral line, which also occurs the short way across the wing disc (Fig. 2b). The second mode,  $Se_1$  (Fig. 5B), repeats the anterior-posterior line. The third mode,  $Ce_2$  (Fig. 5C), has a pair of hyperbolic nodal lines which nicely match the pair of lines separating ventral and dorsal thoracic compartments from the wing compartment lying between them.  $Se_2$  (Fig. 5D) repeats the dorsal-ventral and anterior-posterior lines.  $Ce_3$  (Fig. 5E) draws two nodal hyperbolae near the dorsal and ventral narrow ends of the ellipse. The dorsal member of the pair draws the fourth line separating the dor-

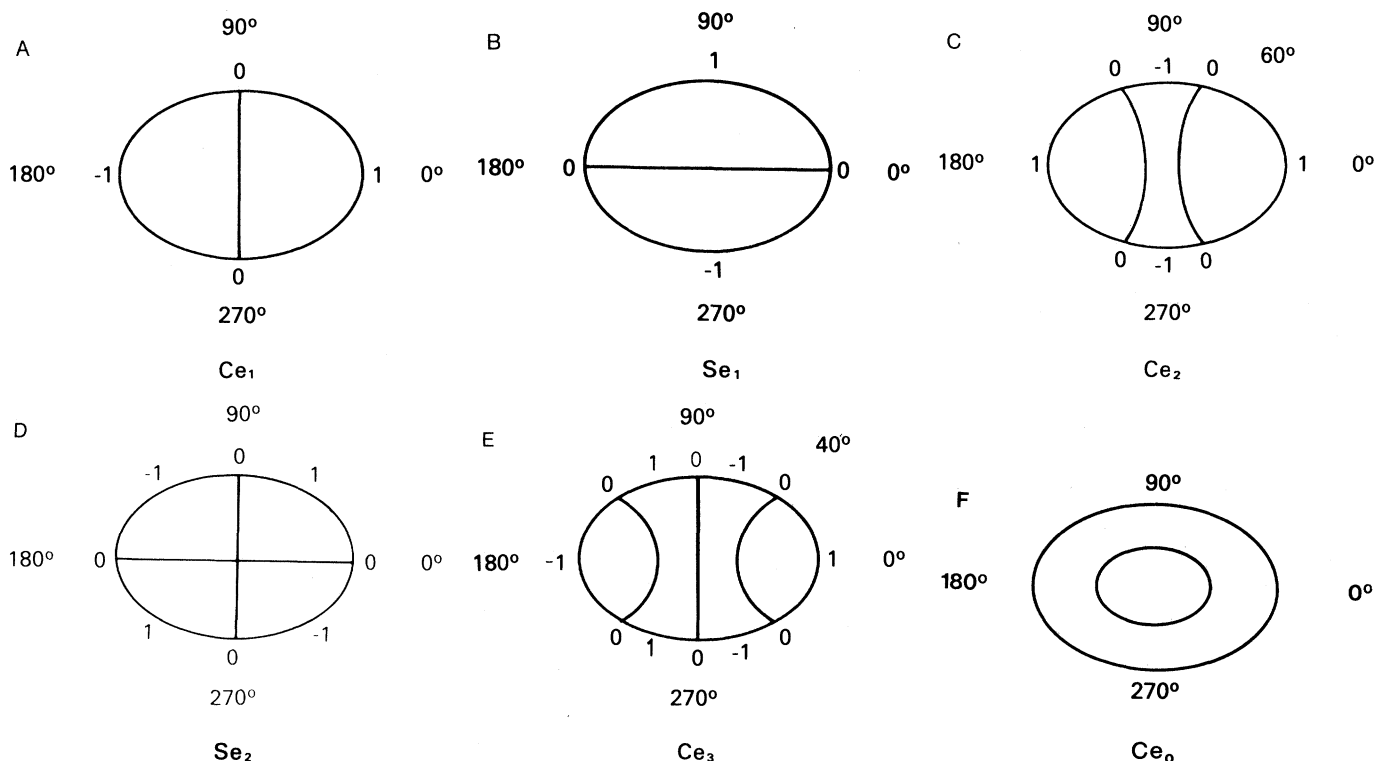


Fig. 5. Nodal lines of successive wave patterns which fit onto an ellipse as it enlarges. The patterns are similar to those on a circle. (A)  $Ce_1(\xi, s_{11})$  ( $\eta, s_{11}$ ) (abbreviated  $Ce_1$ ) is a slight distortion of  $J_1(kr) \cos \phi$  (Fig. 3a). (B)  $Se_1(\xi, s_{11})se_1(\eta, s_{11})$  (that is  $Se_1$ ) is  $Ce_1$  rotated  $90^\circ$ . (C)  $Ce_2$  is analogous to  $J_2(kr) \cos 2\phi$  (Fig. 3b) but on an ellipse the radii split to form pairs of confocal hyperbolae. (D and E)  $Se_2$  and  $Ce_3$  are analogous to  $J_2(kr) \sin 2\phi$  and  $J_3(kr) \cos 3\phi$ , respectively. (F)  $Ce_0(\xi, s_{01})ce_0(\eta, s_{01})$ , or  $Ce_0$  is analogous to  $J_0(kr) \cos 0\phi$ . This mode is a hill-shaped pattern with an interior nodal ellipse, similar to Fig. 3c. See the appendix for definitions of the symbols.

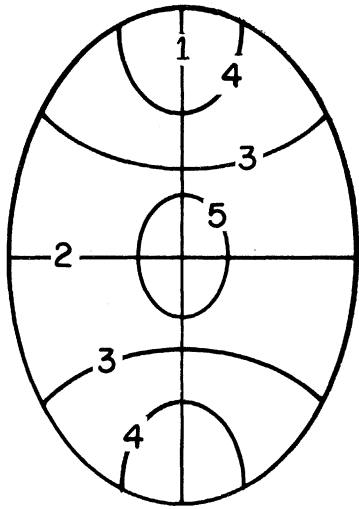


Fig. 6. Taking account of wing disc growth, we project all five predicted compartmental boundaries onto one ellipse. The observed boundaries are shown in Fig. 2b.

sal thorax into scutum-scutellum and postscutum-postscutellum. The ventral member of the pair of hyperbolae is the predicted bisection of ventral thorax needed to complete the twofold symmetry of the observed compartment lines (Fig. 2, a and b). The final "hill" pattern,  $Ce_0$  (Fig. 5F), draws a concentric interior nodal ellipse separating proximal and distal wing.

Taking account of the growth of the wing disc, the predicted compartmental boundaries are summarized in Fig. 6. They compare well to the observed boundaries (Fig. 2b). In short, the sequence, number, position, and symmetries of the second through fifth compartmental boundaries are almost identical to the characteristic chemical patterns arising on a growing ellipse. The compartment lines reflect the symmetries and natural coordinate system of an ellipse.

#### Predictions: Compartment Lines on Other Discs and the Blastoderm

Our model postulates that the chemical patterns occurring in a tissue depend on the tissue's size and shape. It therefore makes testable predictions about sequential compartmentalization on the different, distinctly shaped, imaginal discs and on the ellipsoidal egg.

The compartmental boundaries that form on the leg (4), genital (6), and haltere (11, 29) as well as on the blastoderm (4, 5, 12) are now partially known (Fig. 7, A to C). The occurrence of compartmental boundaries in the eye-antenna disc is in doubt (3, 29).

If the unstable chemical wavelength is

roughly identical in all discs, then the model predicts that the smaller of two discs with homologous shapes should form only the first few of the lines that form on the larger disc. The different imaginal discs fall into two major shape classes. Wing, haltere, and the individual leg discs are convex, fairly symmetric shapes (24, 30). The eye-antenna, genital, and the pair of first leg discs, which are fused, are nonconvex, bilobed structures during most of their development (24, 30). Our model makes distinct predictions for these two shape classes. As predicted, the three lines that form on the smaller haltere disc (29) are homologous to the first three that form on the larger wing disc. The first two on each leg disc match the first two on the larger wing disc. Our model cannot explain the failure of the second leg boundary to extend across the disc. On nonconvex, but symmetrical bilobed structures, one might intuitively expect that a compartmental boundary would form in the narrow isthmus between the lobes. However, none appears to form between the left and right halves of the symmetrical, fused genital disc (6), or between the left and right members of the fused first leg discs (4).

Our model predicts these counterintuitive observations (see the appendix). In symmetrical bilobed structures joined by a sufficiently narrow and short isthmus, the chemical patterns that form must approximately fit in each lobe separately. Thus, chemical patterns with nodal lines across the isthmus, which would create boundaries that isolate one lobe from the other, are suppressed. On the other hand, symmetrical patterns with maxima or minima in the isthmus can form lengthwise along the symmetrical bilobed structure, generating the second compartmental boundaries that arise simultaneously in each lobe of the fused first leg discs, and in each lobe of the fused genital disc.

On the asymmetrical bilobed eye-antenna disc, Baker (3) reports that a longitudinal compartment boundary running through the isthmus divides dorsal eye and dorsal first antennal segment from ventral eye and the rest of the antenna. Later, two lines form at about the same time, perpendicular to the first line, and divide the eye into three regions. The predictions of our model are consistent with this sequence for an appropriate asymmetric bilobed structure. However, other workers (29) have been unable to confirm the occurrence of these compartmental boundaries in the eye-antenna disc.

The most interesting predictions of our

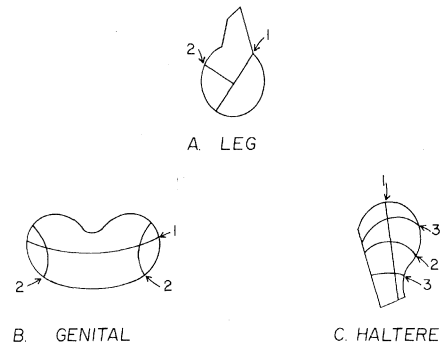


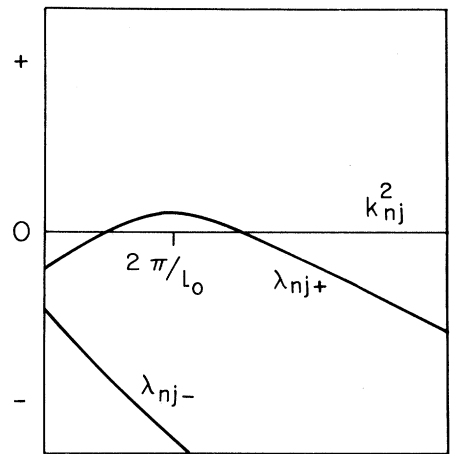
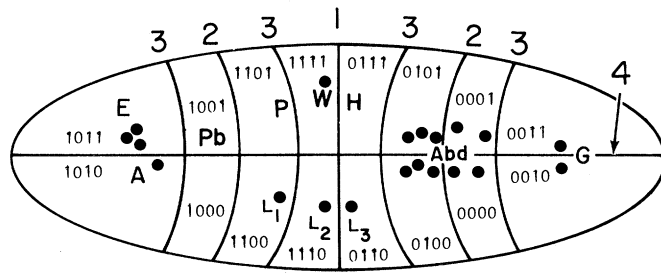
Fig. 7. Schematic compartmental lines on the (A) leg, (B) genital, and (C) haltere.

model concern the forming blastoderm. The egg does not grow during cleavage or later embryogenesis. However, it is likely that, as cell membranes form and separate nuclei, resistance to diffusion increases so that effective diffusion constants are made smaller. If diffusion constants become smaller while the ratios of the diffusion constants do not change, the effect is to shorten the unstable wavelength. Mathematically, the effect is the same as if the unstable wavelength remains constant and the spatial domain grows; as the allowed wavelength becomes shorter, a succession of different patterns fit on the egg at a discrete succession of allowed wavelengths.

A fundamental geometric difference between the cleaving egg and the discs is that the egg is ellipsoidal, whereas the discs are effectively planar. The axis ratio of the egg is about 3.7 to 1 (30). As the allowed wavelength gradually shortens, the patterns that fit on such an ellipsoid arise as longitudinal sinusoidal patterns for the first several allowed discrete wavelengths (26-28). These create circumferential nodal lines, which segment the egg along its length. Only after several longitudinal segments are created is the wavelength short enough to "fit" around the circumference of the egg. Such circumferential patterns will create longitudinal nodal lines, and, on an ellipsoid, the first to arise should divide the dorsal and ventral halves of the egg (Fig. 8). Hence, the model predicts that longitudinal segmentation into at least six, or perhaps more, compartments should occur prior to the establishment of clonal restrictions between dorsal and ventral discs.

As was described earlier, the data now available confirm these predictions. Clones formed at about 3 hours—the blastoderm stage—show restrictions to each of the three thoracic segments, and probably also respect the anterior-posterior compartment lines in the thoracic segments (4, 5, 12). However, clones

Fig. 8 (right). Successive compartmental lines predicted on the fate map (11, 49) of the blastoderm by the chemical wave model, with the binary combinatorial code assignment in each compartment generated by the successive lines. A, antenna; E, eye; Pb, proboscis; Cl, clypeo-labrum; P, prothorax; W, wing and mesothorax; H, haltere; Abd, abdominal segments; G, genital. Assignment of clypeo-labrum to a position below proboscis is tentative. Transdetermination predictions are given in Table 1. Fig. 9 (far right). Qualitative form of the two branches,  $\lambda_{nj+}$  and  $\lambda_{nj-}$ , of the dispersion relation, Eqs. A3, which gives rise to sequential pattern formation. Only those modes with wave number  $k_{nj}$  in the neighborhood of  $2\pi/l_0$  will grow in time and create spatial patterns.



created at this time can run from mesothorax to mesothoracic leg, metathorax to metathoracic leg, and prothorax to prothoracic leg. By 2 hours after the blastoderm stage (12), clones no longer cross between dorsal and ventral discs. Hence, longitudinal segmentation has in fact preceded dorsal-ventral clone restriction, as predicted by our model.

The qualitative predictions of our model are shown in Fig. 8 for the first three longitudinal sinusoidal patterns and the first circumferential pattern. These four patterns create compartmental boundaries that would suffice to separate the major imaginal discs. A fourth longitudinal pattern, analogous to  $Ce_6$ , would simultaneously generate six circumferential compartment boundaries that would form the anterior-posterior disc. As long as it is initially small enough and if it eventually grows larger than required for the final recorded pattern, the locations of nodal compartmental lines will be at the proper locations. We stress that, while the nodal compartmental lines are size-invariant, they are not shape-invariant.

Certain difficulties arise in making detailed predictions about the expected sequence of compartmental lines, tissue sizes at which they occur, and their exact locations. On the wing disc, patterns  $Se_1$  and  $Se_2$  merely repeat previously drawn lines, and therefore the role they might play in compartment formation is not obvious. Dorsal-ventral and wing-thorax boundaries arise at about the same time, while our model predicts an interval of growth between them. On the egg, our linearized equations may predict that the anterior-posterior intrathoracic lines arise after clonal isolation of the dorsal from ventral discs. The wing disc grows 70-fold between the formation of the dorsal-ventral and proximal-distal boundaries, while our model on a perfect ellipse predicts 30-fold growth (Fig. 10). Finally the wing disc

boundaries appear to arise asymmetrically in the disc. Fully nonlinear forms of Eqs. 1 generally have the properties that the expected sequence of chemical patterns can differ from the linear predictions (21, 31, 32); early patterns can, for instance, suppress later patterns; and on the wing disc, for example,  $Ce_1$  and  $Ce_2$  might suppress  $Se_1$  and  $Se_2$ . Also, the nodal lines might be displaced from the locations predicted by the linearized equations (31, 33). An appropriate nonlinear model, coupled with distortions from perfect ellipses and ellipsoids, may therefore be able to circumvent many of the above difficulties. We have limited ourselves to the restrictive predictions of the linearized forms of Eqs. 1.

**Each Compartment May Be Specified by a Binary Combinatorial Code Word**

#### Each Compartment May Be Specified by a Binary Combinatorial Code Word

The first aim of our article has been to account for the sequence and geometries in which compartmental boundaries arise on the blastoderm and imaginal discs. However, our model leads to an interesting hypothesis about the form of developmental commitments in distinct compartments. It is the nodal lines of the successive chemical patterns that appear to correspond to the observed compartmental boundaries. The model's ability to predict the sequence and geometries of "nodal" compartmental lines is independent of how these nodal lines might be recorded. For example, a nodal line might induce special cell junctions or a line of cell death, which thereafter isolates two parts of identical cells. We stress this, since the hypothesis that compartments are distinctly committed cell populations is not conclusively established.

However, it appears highly likely that most compartmental lines do separate groups of cells as a reflection of their commitment to different developmental

Table 1. Predicted relative transdetermination frequencies derived from the chemical wave model applied to the blastoderm.  $L_{1,2} \rightarrow A > L_{1,2} \rightarrow G$  means the model predicts transdetermination from the first or second leg to antenna is greater than to genital. Abbreviations are explained in the legend of Fig. 8.

Prediction	Status	Prediction	Status	Prediction	Status
$H \rightarrow W > H \rightarrow A$	T	$A \rightarrow W > A \rightarrow H$	T	$L \rightarrow W > L \rightarrow E$	T
$H \rightarrow W > H \rightarrow L_{1,2}$	T	$A \rightarrow L > A \rightarrow W$	F	$L_{1,2} \rightarrow W > L_{1,2} \rightarrow H$	T
$H \rightarrow W > H \rightarrow E$	T	$A \rightarrow Pb > G \rightarrow Pb$	?	$L > A > L \rightarrow E$	T
$H \rightarrow W > H \rightarrow Pb$	T	$A \rightarrow E > A \rightarrow W$	F	$L_{1,2} \rightarrow A > L_{1,2} \rightarrow G$	T
$W \rightarrow A > H \rightarrow A$	T	$A \rightarrow G > L_{1,2} \rightarrow G$	T	$L_2 \rightarrow G > L_3 \rightarrow A$	?
$W \rightarrow E > H \rightarrow E$	T	$A \rightarrow E > E \rightarrow A$	T	$L_1 \rightarrow Pb > L_1 \rightarrow G$	?
$W \rightarrow L_{1,2} > H \rightarrow L_{1,2}$	T	$A \rightarrow L_2 > L_2 \rightarrow A$	?T	$G \rightarrow A > G \rightarrow Pb$	T
$W \rightarrow L > W \rightarrow A$	T	$E \rightarrow W > E \rightarrow H$	T	$G \rightarrow A > G \rightarrow W$	T
$W \rightarrow L > W \rightarrow G$	T	$E \rightarrow A > E \rightarrow G$	T	$G \rightarrow L_{2,3} > G \rightarrow W$	?T
$W \rightarrow A > W \rightarrow G$	T	$E \rightarrow A > E \rightarrow L$	T	$G \rightarrow A > G \rightarrow L_{1,2}$	?T
$W \rightarrow E > W \rightarrow Pb$	T	$E \rightarrow W > E \rightarrow L$	T	$G \rightarrow A > A \rightarrow G$	T
$W \rightarrow E > W \rightarrow G$	T			$G \rightarrow L > L \rightarrow G$	T
$W \rightarrow E > W \rightarrow A$	?			$G \rightarrow H > G \rightarrow W$	?F

pathways; therefore, a natural interpretation of our model has been to postulate that the nodal lines of a pattern are a threshold level of a morphogen, which acts to induce one of two different cell choices in cells below or above threshold. By this we are led to suppose that cells in each terminal compartment have recorded the sequence of binary commitments as compartment boundaries form successively. Then each terminal compartment would be named by a unique combination of states of a small number of binary switches (Fig. 8). The possible combinations of states of the several binary switches could properly be thought of as an epigenetic code, each word of which specifies a single compartment.

The geometries of wing disc compartments also suggest that each is specified by a combination of binary names: anterior or posterior, dorsal or ventral, and so on. On the basis of these geometries and an analysis of the homeotic mutants *engrailed*, *bithorax*, and *post-bithorax*, which convert one thoracic compartment to another, Garcia-Bellido (1) and Morata and Lawrence (17) have suggested that each compartment is specified by a combination of several on-off "selector genes."

A binary code (Fig. 8) implies that each switch partitions the discs and disc compartments into two complementary subsets, those where the switch is in state 1 and all the rest, where it is in state 0. If there are genes that act only when

this switch is in state 1 and others that act only when this switch is in state 0, pairs of mutants should exist that affect complementary subsets of discs. Four such pairs are already known (34, 35). They provide independent evidence that each disc is specified by a combination of binary switches (35, 36), and yield a code almost identical to that predicted independently by our chemical pattern model on the blastoderm (Fig. 8) (37).

### Prediction of Transdetermination and Homeotic Transformations

Two highly ordered forms of metaplasia occur in *Drosophila*: transdetermination and homeotic mutations. Transdetermination occurs when an imaginal disc determined to form one appendage is cultured in adult abdomen for several weeks, then injected into a larva for metamorphosis (10, 38). Occasionally, adult cuticle typical of another disc is found in the metamorphosed implant. The patterns of transdetermination frequencies from each disc show that there are sequences of transdeterminations, and there is a global orientation toward thorax (35-38). For example, the transitions genital to antenna to wing to thorax represent one such oriented sequence. Any transdetermination altering one switch should be more frequent than those altering the same switch plus any additional switch. A binary combinatorial code therefore predicts specific sequences of transdetermination as a result of one-step transitions in that code. It also predicts a global orientation of transitions toward the most stable state of each binary switch (35, 36). The particular binary code (Fig. 8) generated by the compartmental lines we predict on the blastoderm yields a large number of specific predictions, most of which are confirmed (Table 1).

For example, transdetermination from haltere to wing should be more frequent than from haltere to antenna, since in both cases the first switch changes from 0 to 1, while in the conversion of haltere to antenna the second and fourth switch must also change from 1 to 0. Of 30 predicted relative frequencies which are unambiguously true or false, only two are false. Four of the 30 predictions reflect a subsidiary assumption that state 1 is more stable than state 0 of each switch, hence that the transition of 0 to 1 is more frequent in each switch than the transition of 1 to 0.

Homeotic mutants convert one tissue to another in highly specific ways (10, 39). If each disc and disc compartment

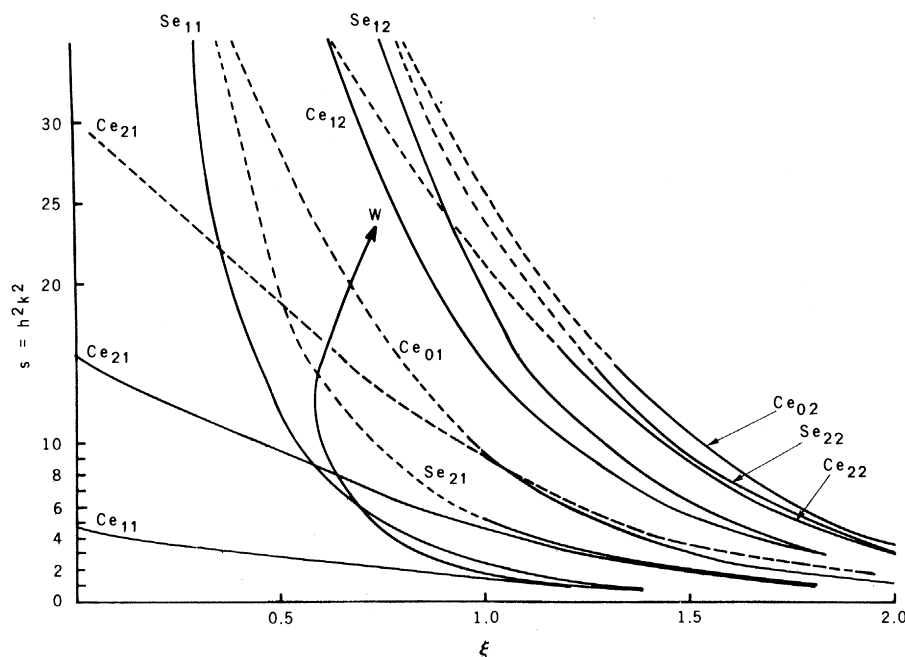


Fig. 10. Two parameters,  $\xi$  and  $s$  (see text), specify all possible ellipses. For all ellipses whose size and shape parameters lie along one of the curves shown, the indicated mode satisfies the no-flux boundary condition with  $k_{nj} = 2\pi/l_0$  and is therefore amplified. The dotted portions of the curves are extrapolations of available data (28). The arrow labeled *W* shows approximate shape changes during growth of the wing disc.

has made a unique combination of binary choices recorded by means of switches, or "selector genes," then some homeotic mutants might convert one compartment to another by altering the state of a single switch. Garcia-Bellido (1) and Morata and Lawrence (17, 40) have already carried out an analysis of the mutants *engrailed*, *bithorax*, and *post-bithorax* on the basis of this idea.

There are at least three general properties predicted of homeosis by a binary code:

(1) In most cases, any given "selector gene" is in the same state in several discs. If a homeotic mutant converts the switch from one to another state in one compartment, it might also do so in other compartments. A *combinatorial* code predicts coordinated homeotic transformations (35, 36).

2) The developmental programs in discs which are geographically distant on the blastoderm can differ in the state of only a single switch (Fig. 8). Thus, some homeotic mutants should transform between tissues widely separated on the blastoderm.

3) If transdetermination in a disc results from altering any one of several switches, but a homeotic mutant alters

the state of a specific switch, then the set of tissues to which one disc can transdetermine should be broader than, but should include, the specific tissue to which one disc is transformed by a homeotic mutant.

Homeotic mutants do exhibit these three general properties (39). Table 2 lists the homeotic mutants that cause transformations between tissues given distinct combinatorial code names in Fig. 8. Many of the mutants involve coordinated transformations of two distinct tissues. In addition, many involve transformations between noncontiguous domains on the blastoderm fate map. Comparison of Tables 1 and 2 confirms that the spectrum of transdeterminations from each disc is broader than, but inclusive of, the effects of a specific homeotic mutant.

If a homeotic mutant acts by altering the states of a binary "selector gene," then an observed homeotic transformation of one tissue to another tissue might require a maximum of four switch alterations in a four digit binary code or a minimum of a single switch alteration. Similarly, if a homeotic causes coordinated transformations of two tissues to two other tissues (parallel transformation),

both might, at a minimum, be due to the simultaneous alteration of the same single switch in the two tissues. However, homeotic transformation of one tissue into two different tissues (divergent transformation), or of two tissues into one tissue (convergent transformations) must require alteration of at least two switches. Table 2 shows that, in our specific binary code in Fig. 8, all but one single and coordinated parallel transformations require only a single switch alteration. All but one of the remaining transformations require the minimum two switch alterations.

The code in Fig. 8 derives from our predicted compartmental boundaries on the blastoderm. If compartmentalization truly reflects binary choices, then a more accurate code should result from an analysis of the actual detailed sequence and geometries of compartment formation in the early embryo. Correlation of such results with the body of data concerning sequential commitment in insect eggs provided by egg ligature, induction of double abdomen phenotypes, and other experiments (20, 48, 50), should not only test our model (51), but provide a more complete understanding of early developmental processes.

Table 2. Observed homeotic transformation, and the code changes required for the code scheme in Fig. 8. A set of homeotic mutants causing the same transformation is represented by one member (10, 39): (1) Antennapedia, Antennapedia, aristapedia, aristatarsia; (2) Ophthalmoptera, ophthalmoptera (44), eyes-reduced; (3) tetraltera, Metaplasia, Haltere mimic; (4) extrasex combs, Extrasexcomb, reduplicated sex comb, sparse arista. Transformations with 1\* and 2\* require one additional switch to account for other transformations of that homeotic.

Mutant	Symbol	Transformation	Coordination	Code Change	Switches Required	Ref
Antennapedia <sup>(1)</sup>	Antp	antenna → leg 2	-	1010→1110	1	10, 39
Pointed wing	Pw	antenna → wing	-	1010→1111	2	39
Nasobemia	Ns	antenna → leg 2	parallel	1010→1110	1	44
		eye → wing				
dachsous	ds	tarsus → arista	-	1110→1010	1	39
Ophthalmoptera <sup>(2)</sup>	OptG	eye → wing	-	1011→1111	1	39
Hexaptera	Hx	prothorax → mesothorax	-	1101→1111	1	39
podoptera	pod	wing → leg	-	1111→1110	1	39
tetraltera <sup>(3)</sup>	tet	wing → haltere	-	1111→0111	1	39
Contrabithorax	Cbx	wing → haltere	parallel	1111→0111	1	39
		leg 2 → leg 3				
Ultrabithorax	Ubx	haltere → wing	parallel	0111→1111	1	43
		leg 3 → leg 2				
tumorous head	tuh1,3	eye → genital	parallel	1011→0011	1	47
		antenna → genital				
		antenna → leg	divergent	1010→1110	1*	47
lethal(3) III-10	1(3) III-10	haltere → wing	parallel	0111→1111	1	34
lethal(3) XVI-18	1(3) XVI-18	genital → antenna				
		genital → leg	divergent	0010→1010	1	39
		genital → leg	divergent	0010→0110	1*	34
lethal(3) 703	1(3) 703	antenna → leg	parallel	1010→1110	1	34
lethal(3) 1803R	1(3) 1803R	genital → leg				
		genital → antenna	divergent	0010→0110	1	39
		genital → antenna	divergent	0010→1010	1*	39
		haltere → wing	parallel	0111→1111	1	39
proboscipedia	pb	proboscis → antenna	divergent	1000→1010	1	10
		proboscis → leg				
extrasexcombs <sup>(4)</sup>	ecs	leg 2 → leg 1	convergent	1110→1100	1	39
		leg 3 → leg 1				
Polycomb	Pc	antenna → leg 2	-	1010→1110	1	39
lethal(4) 29	1(4) 29	leg 2 → leg 1	convergent	1110→1100	1*	10
		leg 3 → leg 1				
		leg 3 → leg 1	convergent	0110→1100	2*	39

## Conclusion

During development of *Drosophila melanogaster*, sequential commitment to alternative developmental programs occurs in neighboring groups of cells, and probably is reflected by formation of compartmental boundaries which progressively subdivide the early embryo and later the imaginal discs. The reasonable success of our chemical pattern model in predicting the locations and temporal order of compartmental boundaries, may lead to other projects showing that a uniform mechanism may act throughout development to determine the locations of successive developmental commitments. The success of the binary combinatorial code generated by the chemical patterns in accounting for transdetermination and homeotic mutants not only underscores the possibility that the logic of developmental commitments in *Drosophila* is written in a binary code, but also it yields a new view of sequential commitments in early embryogenesis, which is open to experimental tests.

## Appendix

This section deals with the analysis of the reaction-diffusion system.

In the chemical system (Eqs. 1), spatial patterns can spontaneously arise from an initial spatially homogeneous concentration profile by the selection from noise and amplification of perturbations with wavelengths in the neighborhood of some preferred wavelength. To determine the conditions under which this occurs, the behavior of the system in the vicinity of the spatially homogeneous steady state,  $X = X_0$ ,  $Y = Y_0$ , where  $F(X_0, Y_0) = G(X_0, Y_0) = 0$ , is analyzed using a standard linearization procedure.

The system (Eqs. 1) is linearized about the spatially homogeneous steady state by substituting  $X(\mathbf{r}, t) = X_0 + x(\mathbf{r}, t)$ ,  $Y(\mathbf{r}, t) = Y_0 + y(\mathbf{r}, t)$ , and retaining only terms up to first order in  $x$  and  $y$  in a Taylor expansion of  $F(X, Y)$  and  $G(X, Y)$ . The resulting linear equations in  $x$  and  $y$  are

$$\begin{aligned} \partial x / \partial t &= K_{11}x + K_{12}y + D_1 \nabla^2 x \\ \partial y / \partial t &= K_{21}x + K_{22}y + D_2 \nabla^2 y \end{aligned} \quad (\text{A1})$$

These equations are solved by separating out the time dependence through the substitutions  $x(\mathbf{r}, t) = x'(\mathbf{r})e^{\lambda t}$ ,  $y(\mathbf{r}, t) = y'(\mathbf{r})e^{\lambda t}$ , and diagonalizing the resulting pair of spatially dependent coupled equations. These two separated equations are Helmholtz-type equations whose solu-

tions can be straightforwardly obtained in different coordinate systems (23, 25). The complete space-time dependent solutions are sums of spatial modes or patterns, each with a characteristic temporal behavior. For example, the complete solution on a circle can be written

$$\begin{bmatrix} x(r, \phi, t) \\ y(r, \phi, t) \end{bmatrix} = \sum_{i=+,-} \sum_{j=1}^{\infty} \sum_{n=0}^{\infty} \begin{bmatrix} a_{nji} \\ b_{nji} \end{bmatrix} \times \exp \lambda_{nji} t J_n(k_{nj}r) \cos n\phi \quad (\text{A2})$$

where  $J_n$  is the  $n^{\text{th}}$  Bessel function and  $r$  and  $\phi$  are the radial and angular coordinates, respectively.  $a_{nji}$  and  $b_{nji}$  are arbitrary constants to be determined by initial conditions. Each mode has two temporal eigenvalues, indicated by the sum  $i = +, -$ . The sum over  $j$  depends on the boundary conditions chosen.

For no-flux boundary conditions, the spatial gradient at the boundary must have zero component normal to the boundary (23). In a circle of radius  $r_0$ , this means that  $\partial x(r, \phi, t) / \partial r = \partial y(r, \phi, t) / \partial r = 0$  at  $r = r_0$ . The zeros in the derivatives of  $J_n(z)$  occur at particular values of the argument  $z = z_{nj}$  (26). Therefore, the spatial mode  $J_n(k_{nj}r) \cos n\phi$ , which we abbreviate by  $J_{nj}$ , is obtained when the  $j^{\text{th}}$  zero in the derivative of  $J_n$  occurs at the boundary; that is, when  $k_{nj}r_0 = z_{nj}$ . This fixes the value of  $k_{nj}$  associated with the mode  $J_{nj}$  for any given radius  $r_0$ . As the radius changes, the value of  $k_{nj}$  changes in inverse proportion.

The temporal behavior of the mode  $J_{nj}$  is determined by the dynamics through the dispersion relation between the temporal eigenvalues  $\lambda_{nji}$  and the spatial eigenvalue  $k_{nj}$ . For Eqs. A1 this relation has the form

$$\begin{aligned} \lambda_{nj\pm} &= \frac{1}{2} \left[ K_{11} + K_{22} - k_{nj}^2(D_1 + D_2) \right. \\ &\quad \left. \pm \{ [K_{11} - K_{22} - k_{nj}^2(D_1 - D_2)]^2 \right. \\ &\quad \left. + 4K_{12}K_{21} \}^{1/2} \right] \end{aligned} \quad (\text{A3})$$

As seen in Eq. A2, each mode  $J_{nj}$  behaves in time according to a sum of terms of the form  $A \exp \lambda_{nj+} t + B \exp \lambda_{nj-} t$ , where  $A$  and  $B$  are specified by initial conditions. Therefore, any mode with the real parts of  $\lambda_{nj+}$  and  $\lambda_{nj-}$  both negative will decay and disappear; a mode with either or both real parts positive will grow and create a spatial pattern.

On an ellipse, the solutions of Eq. A1 are

$$\begin{bmatrix} x(\xi, \eta, t) \\ y(\xi, \eta, t) \end{bmatrix} = \sum_{i=+,-} \sum_{j=1}^{\infty} \sum_{n=0}^{\infty} \begin{bmatrix} a_{nji} \\ b_{nji} \end{bmatrix} \times \exp \lambda_{nji} t [C e_n(\xi, s_{nj}) c e_n(\eta, s_{nj}) + S_{nji} S e_n(\xi, s_{nj}) s e_n(\eta, s_{nj})] \quad (\text{A4})$$

Here  $c e_n$  and  $s e_n$  are periodic cosine- and sine-elliptic Mathieu functions, respectively, of integral order and  $C e_n$  and  $S e_n$  are the corresponding nonperiodic (or modified) Mathieu functions (25).  $\xi$  and  $\eta$  are the elliptical coordinates tracing out confocal ellipses and hyperbolae, respectively (Fig. 4), and  $s_{nj} = h^2 k_{nj}^2$ , where  $h$  is one-half the interfocal distance of the ellipse. The constants  $a_{nji}$ ,  $b_{nji}$ , and  $S_{nji}$  are determined by initial conditions. We use the abbreviations  $C e_{nj}$  or  $S e_{nj}$  for the patterns  $C e_n(\xi, s_{nj}) c e_n(\eta, s_{nj})$  or  $S e_n(\xi, s_{nj}) s e_n(\eta, s_{nj})$ , respectively.

At the boundary of the ellipse,  $\xi = \xi_0$ , the no-flux condition becomes  $\partial C e_n(\xi, s_{nj}) / \partial \xi = 0$  or  $\partial S e_n(\xi, s_{nj}) / \partial \xi = 0$ , analogous to the circular case. This condition fixes the value of the scaling factor  $k_{nj}$  for the pattern  $C e_{nj}$  or  $S e_{nj}$ , and the temporal behavior of this pattern is determined by exactly the same dispersion relation (Eq. A3) as for the circular case. Those modes which grow in time will form spatial patterns on the ellipse; those which decay in time will not be seen.

If the following five conditions hold

- (i)  $K_{11} + K_{22} < 0$
- (ii)  $K_{11}K_{22} - K_{12}K_{21} > 0$
- (iii)  $(K_{11} - K_{22})^2 > -4K_{12}K_{21}$
- (iv)  $D_1K_{22} + D_2K_{11} > 0$
- (v)  $\left( \sqrt{\frac{D_1}{D_2}} K_{22} - \sqrt{\frac{D_2}{D_1}} K_{11} \right)^2 > -4K_{12}K_{21}$  (A5)

spatial patterns will arise spontaneously. In such a system, one reactant diffuses more readily than the other, one catalyzes its own production while the other inhibits its own production, and one catalyzes the production of the second while the second inhibits the production of the first. Under these conditions, the temporal eigenvalues  $\lambda_{nj+}$  and  $\lambda_{nj-}$  will both be real and the larger of them,  $\lambda_{nj+}$ , will be positive only in the neighborhood of a particular value of  $k_{nj}$ , equal to  $2\pi/l_0$ , where  $l_0$  is the natural chemical wavelength of the system (Fig. 9). Since only those modes with positive  $\lambda_{nj+}$  are amplified, only that pattern  $C e_{nj}$  or  $S e_{nj}$  will grow which satisfies the no-flux boundary condition with  $k_{nj} \approx 2\pi/l_0$ . Furthermore, since  $\lambda_{nj+}$  is real, this pattern will grow without oscillation.

For an ellipse with a given eccentricity  $\epsilon = 1/\cosh \xi_0$ , the wave number  $k_{nj}$  for the pattern  $C e_{nj}$  or  $S e_{nj}$  is inversely proportional to the interfocal distance,  $2h$ , and therefore to the size of the ellipse (25), in direct analogy with the circular case. Therefore as the size increases, each  $k_{nj}$  will be scaled downward along

the abscissa in Fig. 9, and different modes will appear in sequence as their respective  $k_{nj}$ 's enter the region of positive  $\lambda_{nj+}$ . However, since more and more modes will be compressed into the region of small  $k_{nj}$ , eventually more than one mode will fall in the positive  $\lambda_{nj+}$  region. In this case, a superposition of modes might appear or, in a fully nonlinear system, a previously established mode might suppress a later mode even though both are allowed in the linear theory.

The particular pattern selected depends not only on the size of the ellipse, but also on its eccentricity or shape. In Fig. 10 we show a two-parameter space of all possible ellipses. The abscissa  $\xi$  specifies the eccentricity of the ellipse,  $\cosh \xi = 1/\epsilon$ , and the ordinate specifies the parameter  $s = h^2 k^2$ , where  $2h$  is the interfocal distance and the subscripts have been dropped. Since all allowed patterns have the same value of  $k$  ( $= 2\pi/l_0$ )  $s$  depends only on  $h^2$ , and therefore is a direct measure of the size of the ellipse. The lines labeled  $Ce_{nj}$  or  $Se_{nj}$  are the loci along which the indicated mode satisfies the no-flux boundary condition with  $k_{nj} = 2\pi/l_0$  (28). The dotted portions of the lines are our extrapolations of the available data. Changes in size and shape of a smoothly growing ellipse can be plotted as a continuous trajectory in Fig. 10. Whenever such a trajectory intersects one of the mode lines, that mode will be selected and amplified. Therefore, the sequence of patterns that arise is determined by the sequence in which the mode lines are crossed by the growth trajectory. Note that since the region of amplification in Fig. 9 has a finite size, a given mode can be amplified in a small region on either side of its indicated mode line. If two mode lines are near one another both may be allowed in the linear theory, and superposition of the two or suppression of one by the other could occur.

The curve labeled W in Fig. 10 shows an estimate of the size and shape changes which occur in the growing wing disc, approximating it as a perfect ellipse (24). The predicted sequence of modes is  $Ce_{11}$ ,  $Se_{11}$ ,  $Ce_{21}$ ,  $Se_{21}$ ,  $Ce_{31}$ , and  $Ce_{01}$ . The final subscripts are dropped in the text.

In the linear approximation given by Eqs. A1, modes selected for amplification grow without bound. The nonlinear reaction-diffusion system

$$\frac{\partial X}{\partial t} = -AX + \frac{BY^n}{1+Y^n} + D_1 \nabla^2 X$$

$$\frac{\partial Y}{\partial t} = -CY + \frac{D(Y^n + b)}{1+Y^n} + D_2 \nabla^2 Y \quad (\text{A6})$$

is an example of a system which can create spatial patterns as described above, but in which these patterns grow only to a finite size. In this system,  $X$  inhibits both its own and  $Y$ 's production, and  $Y$  catalyzes the production of both. Also,  $X$  diffuses more readily than  $Y$ .

In Eqs. A6, with  $A = 7.8$ ,  $B = 15.6$ ,  $C = 1$ ,  $D = 1.7$ ,  $b = 0.2$ ,  $n = 6$ ,  $D_1 = 16$ ,  $D_2 = 1$ , this system has one spatially homogeneous steady state at  $X_0 = Y_0 = 1$ . Linearizing about this steady state and substituting the resulting linearization constants  $K_{ij}$  into the dispersion relation, Eq. A3, we find that  $\lambda_{nj+}$  is positive for  $k_{nj}$  between 0.7 and 1.0, corresponding to wavelengths between  $l_{\min} = 6.1$  and  $l_{\max} = 9.1$ . In a one-dimensional domain  $0 < r < L$ , the linearization of Eqs. A6 would therefore amplify the pattern  $\cos n\pi r/L$  henceforth called the "n-model," in the range of lengths  $1/2nl_{\min} < L < 1/2nl_{\max}$ . Computer simulations showed that the analogous nonlinear patterns appeared in the identical length ranges, although their shapes were slight distortions of pure cosines.

In symmetrical bilobed domains, represented by two identical rectangles joined by a short narrow isthmus, the even lengthwise modes, with antinodes at the join, appeared at the same overall lengths as for the one-dimensional case.

The range of lengths supporting the one-mode was compressed and shifted downward toward zero as the join was made narrower. The range of each higher odd mode shifted downward, overlapped that of the even mode below, and finally became coincident with the even mode's range in the limit of a very narrow join. These conditions tend to suppress the antisymmetrical modes if tissue growth is rapid enough, since the first antisymmetrical mode could well be skipped entirely, and each symmetrical mode will become established and may not fully decay before growth has taken the system beyond the range of the overlapping antisymmetrical mode.

For nonsymmetric bilobed shapes (with unequal rectangles) simulations showed that all lengthwise modes tended to appear at somewhat shorter overall lengths than their one-dimensional counterparts. However, the exact sequence of modes depends critically on the geometry, making predictions difficult.

#### References and Notes

1. A. Garcia-Bellido, *Ciba Found. Symp.* **29**, 161 (1975).
2. P. Ripoll, G. Morata, *Dev. Biol.* **48**, 132 (1976).
3. W. Baker, in preparation.
4. E. Steiner, *Arch. Entwickl. Org.* **180**, 9 (1976).
5. E. Wieschaus and W. Gehring, *Dev. Biol.* **50**, 249 (1975).

6. K. Dubendorfer, thesis, University of Zurich (1977).
7. F. H. C. Crick and P. A. Lawrence, *Science* **189**, 340 (1975).
8. F. R. Turner and A. P. Mahowald, *Dev. Biol.* **50**, 95 (1976).
9. L. J. Chan and W. Gehring, *Proc. Natl. Acad. Sci. U.S.A.* **68**, 2217 (1971); K. Illmensee, *Arch. Entwickl. Org.* **170**, 267 (1972).
10. R. Nothiger and W. Gehring, in *Developmental Systems II: Insects*, S. Counce and C. H. Waddington, Eds. (Academic Press, New York, 1973), p. 161.
11. A. Garcia-Bellido and J. R. Merriam, *J. Exp. Zool.* **170**, 1 (1969).
12. P. Lawrence and G. Morata, *Dev. Biol.* **56**, 40 (1977).
13. G. Morata and P. Ripoll, *ibid.* **42**, 221 (1975).
14. P. Bryant, *Ciba Found. Symp.* **29**, 71 (1975); P. Bryant, *J. Exp. Zool.* **193**, 49 (1975).
15. J. Haynie and P. Bryant, *Nature (London)* **259**, 659 (1976).
16. G. Morata, *J. Embryol. Exp. Morphol.* **34**, 19 (1975); A. Garcia-Bellido and P. Santamaria, *Genetics* **72**, 87 (1972).
17. G. Morata and P. A. Lawrence, *Nature (London)* **255**, 614 (1975); ———, *ibid.* **265**, 211 (1977).
18. A. M. Turing, *Philos. Trans. R. Soc. London, Ser. B* **237**, 37 (1952).
19. J. I. Gmitro and L. E. Scivin, in *Intracellular Transport*, K. B. Warren, Ed. (Academic Press, New York, 1966).
20. H. Meinhardt, *J. Cell Sci.* **23**, 117 (1977).
21. G. Nicolis and I. Prigogine, *Self-Organization in Nonequilibrium Systems* (Interscience, New York, 1977).
22. For reaction times  $\tau$  of the order of 100 seconds and diffusion constants of the order of  $10^{-6}$  cm<sup>2</sup>/sec, the characteristic "diffusion length" of the system is  $(D\tau)^{1/2} = 100 \mu\text{m}$ .
23. P. M. Morse and H. Feshbach, *Methods of Theoretical Physics* (McGraw-Hill, New York, 1953).
24. C. Auerbach, *Trans. R. Soc.* **58**, 787 (1933); M. Madhavan, personal communication.
25. N. W. McLachlan, *Theory and Applications of Mathieu Functions* (Clarendon, Oxford, 1947).
26. M. Abramowitz and I. A. Stegun, *Handbook of Mathematical Functions* (Government Printing Office, Washington, D.C., 1972).
27. E. Jahnke, F. Emde, F. Lusch, *Table of Higher Mathematical Functions* (McGraw-Hill, New York, 1960).
28. M. J. King and J. C. Wiltse, *Derivative Zeros and Other Data Pertaining to Mathieu Functions* (Johns Hopkins Radiation Laboratory Technical Report No. AF57, Baltimore, Md., 1958).
29. G. Morata, personal communication.
30. M. Demerec, *The Biology of Drosophila* (Wiley, New York, 1950).
31. Simulating a fully nonlinear model with a natural wavelength in a growing one-dimensional domain, Harrison and Lacalli (personal communication) found that after the first half-wavelength asymmetrical mode, several symmetrical modes appeared. We assume that on the egg, patterns analogous to  $Ce_1$ ,  $Ce_2$ ,  $Ce_3$ , and  $Ce_6$  form in succession.
32. A. Babloyantz and J. Hierneux, *J. Math. Biol.* **37**, 637 (1975).
33. M. Herschkowitz-Kaufman, *Bull. Math. Biol.* **37**, 589 (1975).
34. A. Shearn, T. Rice, A. Garen, W. Gehring, *Proc. Natl. Acad. Sci. U.S.A.* **68**, 2594 (1971).
35. S. A. Kauffman, *Science* **181**, 310 (1973).
36. ———, *Ciba Found. Symp.* **29**, 201 (1975).
37. ———, *Am. Zool.* **17**, 631 (1977).
38. E. Hadorn, in *Major Problems in Developmental Biology*, M. Locke, Ed. (Academic Press, New York, 1966), p. 85.
39. W. J. Ouweneel, *Adv. Genet.* **18**, 179 (1976).
40. P. Lawrence and G. Morata, *Dev. Biol.* **50**, 321 (1976).
41. W. J. Ouweneel, *Acta Embryol. Exp.* **95**, 119 (1970).
42. E. B. Lewis, *Drosophila Inform. Serv.* **30**, 130 (1956); P. Roberts, *Genetics* **49**, 593 (1964).
43. E. B. Lewis, in *The Role of the Chromosomes in Development*, M. Locke, Ed. (Academic Press, New York, 1964).
44. W. J. Gehring, *Arch. Julius Klaus-Stift. Vererbungsforsch. Sozialanthropol. Rassenhyg.* **41**, 44 (1966).
45. V. P. Stepshin and E. K. Ginter, *Genetika* **8**, (8), 93 (1972).
46. A. L. Bull, *J. Exp. Zool.* **161**, 221 (1966).
47. J. H. Postlethwait, P. Bryant, G. Schubiger, *Dev. Biol.* **29**, 337 (1972).
48. G. Schubiger, R. C. Moseley, W. J. Wood, *Proc. Natl. Acad. Sci. U.S.A.* **74**, 2050 (1977).

49. Y. Hotta and S. Benzer, *ibid.* 73, 4154 (1976).  
 50. K. Sander, *Adv. Insect Physiol* 12, 125 (1976).  
 51. Ligation of *Drosophila* and other insect eggs at progressively later cleavage stages causes a progressively narrower gap of missing larval or adult structures centered about the line of ligation (48, 50). The bicaudal mutant of *Drosophila*

produces mirror image abdomen with all or only the posterior few segments (46, 50). Similar double abdomen in *Smittia* can be produced by puncture or irradiation of the anterior egg pole (50). Elegant single and double gradient models (20, 50) have been proposed to account for these phenomena. Although our model was not constructed with these data in mind, it can predict at

least their major qualitative features. We shall discuss this in detail elsewhere.

52. Supported in part by grants from the National Institutes of Health (1-R01-GM-22341-01 and the National Science Foundation (BMS-75-11917). Part of this work was done while S.K. and K.T. were at the Laboratory of Theoretical Biology, National Cancer Institute.

## Science Centers: A Potential for Learning

Science centers are educational institutions designed around informal learning activities.

Lee Kimche

Science centers provide a whole new field of self-motivating experiences in learning, through environmental exhibits that appeal to the senses, emotions, and intellect. They are among the most rapidly developing institutions of learning in

praisal; perhaps some of the methods used in science centers can be adapted to enhance more conventional methods of teaching.

The growth of science centers began early in the century. The greatest growth

---

*Summary.* The past decade has witnessed a proliferation of science-technology centers, or public places for informal learning about science and technology. Science centers are the only institutions that can provide the general public with participatory exhibits and experiences, together with an accurate scientific interpretation of the materials that are involved. The dramatic rise in attendance and the enthusiasm of repeat visitors to science centers reflect a strong public demand for exhibits designed to help the visitor develop a better understanding of the contemporary scientific issues of society.

---

contemporary society. They have been responsive to a growing public demand for knowledge and information. As more and more people visit them, the science centers have a unique opportunity to assist a large segment of the public to gain a greater understanding of the contemporary technological issues of society. The objects and exhibits can form the basis for other types of educational programs, not only within museums, but throughout the entire community. The informal educational techniques that science centers employ may have implications for other types of institutions. Traditional forms of education are undergoing reap-

has occurred within the last 10 years, and there is no sign that the trend will slow down soon. The expansion of existing science centers is proceeding apace with the building of new facilities.

### Attendance Explosion at Science Centers

The increasing number and size of science centers is a direct result of the sharp rise in public demand on existing institutions. The number of visitors to science museums is greater than to any other single type of museum. According to a 1974 survey of 1820 institutions conducted by the National Endowment for the Arts (1), 38 percent of all museum visits were to science museums, 24 percent to history museums, and 14 percent

to art museums. The survey, which included natural history museums in the science museum category, found that, of a total of 308 million museum visits in FY 1971-72, 117 million were to science museums. Excluding natural history museums, science-technology centers alone have experienced skyrocketing attendance in this decade, with the 14.4 million visits registered in 1973 soaring to 36.5 million in 1975. And in 1976, more than one-fifth of the members of the Association of Science-Technology Centers reported attendance increases of at least 10 percent since 1975. Many science centers that offer after-school, evening, weekend, and summer courses have reported waiting lists for enrollment, and still other museums have been forced to impose time limits at certain participatory exhibits due to long waiting lines.

Until recently, it was thought that science centers appealed primarily to children. It is true that school groups form approximately 25 percent of visitors to these centers, but a brief survey shows that 45 percent of the visitors are adults, including college students and senior citizens (2).

Most full-scale science-technology centers offer workshops for all age groups in chemistry, biology, photography, ham radio operations, computers, magnetism, model airplane construction, and other popular fields. Classes and workshops for school-age children reveal some intriguing offerings, such as "Elementary, My Dear Watson: Solving Problems by Deduction," "Marble Shoot Computers," "Water Wizardry," "Optical Toys and Parlor Amusements," and "Performing Plants." Although fewer programs are offered for adults, they range from auto rally classes to lapidary labs, from workshops on dehydrating foods to "Wild Parties," banquets based on edible wild plants (3).

### Characteristics of Science Centers

Most other kinds of museums have evolved as depositories for categorical collections that may be admired by the public and studied by scholars in private. While traditional museums emphasize static displays of objects and artifacts,

---

The author was executive director of the Association of Science-Technology Centers in Washington, D.C. She is now director of the Institute of Museum Services, U.S. Department of Health, Education, and Welfare, Washington, D.C.